Random sequential adsorption of self-avoiding chains on two-dimensional lattices

L. S. Ramirez [*]
Departamento de Física, Instituto de Física Aplicada, Universidad Nacional de San Luis-CONICET, Ejército de Los Andes 950, D5700HHW, San Luis, Argentina
and Instituto de Física Interdisciplinar y Sistemas Complejos, IFISC (CSIC-UIB), Campus Universitat Illes Balears, E-07122 Palma de Mallorca, Spain

P. M. Pasinetti [†] and A. J. Ramirez-Pastor [‡]
Departamento de Física, Instituto de Física Aplicada, Universidad Nacional de San Luis-CONICET, Ejército de Los Andes 950, D5700HHW, San Luis, Argentina

(Received 5 December 2022; revised 30 April 2023; accepted 12 May 2023; published 5 June 2023)

Random sequential adsorption of extended objects deposited on two-dimensional regular lattices is studied. The depositing objects are chains formed by occupying adsorption sites on the substrate through a self-avoiding walk of k lattice steps; these objects are also called "tortuous k-mers." We study how the jamming coverage, $\theta_{j,k}$, depends on k for lattices with different connectivity (honeycomb, square, and triangular). The dependence can be fitted by the function $\theta_{j,k} = \theta_{j,k\to\infty} + B/k + C/k^2$, where B and C are found to be shared parameters by the three lattices and $\theta_{j,k\to\infty}$ (>0) is the jamming coverage for infinitely long k-mers for each of them. The jamming coverage is found to have a growing behavior with the connectivity of the lattice. In addition, $\theta_{j,k}$ is found to be higher for tortuous k-mers than for the previously reported for linear k-mers in each lattice. The results were obtained by means of numerical simulation through an efficient algorithm whose characteristics are discussed in detail. The computational method introduced here also allows us to investigate the full-time kinetics of the surface coverage $\theta_k(t)$ [$\theta_{j,k} \equiv \theta_k(t \to \infty)$]. Along this line, different time regimes are identified and characterized.

DOI: 10.1103/PhysRevE.107.064106

I. INTRODUCTION

The adsorption (or deposition) of particles on solid surfaces is a challenging theoretical problem with important applications related to thin surface films. Using equilibrium statistical mechanics, numerous studies have been carried out on the problem of reversible adsorption [1]. However, in many experiments on adhesion of colloidal particles and proteins on solids substrates, the relaxation timescales are much longer than the times of the formation of the deposit. This situation has encouraged the scientific community to explore research on irreversible adsorption [2].

In the most common picture for systems out of equilibrium, the change of state of surface sites from empty or vacancy to filled or occupied (or vice versa) occurs randomly, sequentially, and irreversibly. This process is known as random sequential adsorption (RSA) [3–6], and has been applied to a large number of systems where the deposition of objects is irreversible over timescales of physical interest. Among others, a variety of biological [3], physical [7], chemical [8], and ecological [9] processes have been modeled by using an RSA scheme.

The assumptions of the RSA models are easily stated: objects are placed randomly one after another in a d-dimensional volume [4]. In the case that the last placed object overlaps with any of those already present, it is immediately removed; otherwise its position is permanently fixed. The scheme is applied to model objects of different shapes and sizes deposited on a discrete or continuous surface [10–16]. The quantity of interest is the fraction of surface, $\theta(t)$, covered in time, t, by the depositing particles or objects. Under these conditions, each deposited particle affects the geometry of all later placements. Thus, the dominant effect in RSA is the blocking of the available substrate area, and the limiting (jamming) coverage $\theta_j = \theta(t \to \infty)$ is less than in close packing.

In the framework of the RSA and discrete models (which is the topic of this paper), several authors investigated the isotropic deposition of straight rigid k-mers on two-dimensional (2D) square lattices [17–20]. In Ref. [17], linear k-mers with k between 2 and 512 were randomly and isotropically deposited on a 2D square lattice. By using computer simulations, the authors found that the jamming concentration monotonically decreases and tends to 0.660(2) as the length of the rods increases. Bonnier *et al.* [17] reported that the jamming coverage as a function of size k follows a law $\theta_{j,k} = 0.660 + 1.071/k - 3.47/k^2$ ($k \geqslant 48$).

Kondrat and Pekalski [18] extended the study to longer objects ($2 \leqslant k \leqslant 2000$) and corroborated that, as reported by Bonnier *et al.* [17], the jamming coverage decreases

[*] luciaramirez@ifisc.uib-csic.es
[†] mpasi@unsl.edu.ar
[‡] antorami@unsl.edu.ar

monotonically approaching the asymptotic value of $\theta_{j,k\to\infty} = 0.66(1)$ for large values of k. In Ref. [18], a power law was reported for θ_j vs k: $\theta_{j,k} = 0.66 + 0.44k^{-0.77}$. Recently, Slutskii *et al.* [19] obtained the percolation thresholds and jamming concentrations for lengths of k-mers up to 2^{17}.

In the case of triangular lattices, the jamming problem corresponding to straight rigid k-mers was studied in Ref. [21]. Using values of k between 2 and 20, the authors found that $\theta_{j,k\to\infty} = 0.56(1)$. Later Perino *et al.* [22] extended the analysis to larger lattices and longer objects: $2 \leqslant k \leqslant 128$ and $L/k = 100, 150, 200, 300$. The results obtained showed that the jamming coverage decreases monotonically approaching the asymptotic value of 0.5976(5) for large values of k: $\theta_{j,k} = 0.5976 + 1.268/k - 3.61/k^2$ ($k \geqslant 12$). The finding in Ref. [22] improves previous estimate in Ref. [21], showing the advantages of having reached larger k-mer sizes.

More recently [23], the RSA of linear k-mers on honeycomb lattices was investigated for k ranging between 2 and 128. Following the procedure in Refs. [17,22], simulation data were fitted by the function $\theta_{j,k} = A + B/k - C/k^2$. In this case, $A = 0.6007(6)$, $B = 1.84(5)$ and $C = 8.36(70)$ ($k \geqslant 16$). The value of A represents the limit concentration by infinitely long k-mers: $\theta_{j,k\to\infty} = A = 0.6007(6)$.

The jamming behavior of objects that have any shape is more complex than the linear one. In the square lattice, the deposition of different objects has been studied: squares [3,24–32], rectangles [33], T-shaped objects and crosses [34], ring polymer chains [35], etc. Y-shaped particles and tetrominoes have also been investigated in honeycomb lattices [36,37]. With respect to triangular lattices, Budinski-Petković *et al.* [21,38–40] examined the kinetics of the RSA of objects of various shapes (linear segments, angled objects, triangles, and hexagons) on homogeneous lattices [21,38,39] and lattices with quenched impurities [40]. The coverage of the surface and the jamming limits were calculated by Monte Carlo (MC) simulation. In all cases, the authors found that the jamming coverage decreases monotonically as the k-mer size increases: $\theta_{j,k} = \theta_0 + \theta_1 \exp(-k/r)$, where θ_0, θ_1, and r are parameters that depend on the shape of the adsorbing object. The deposition of more complex shapes, made by self-avoiding lattice steps whereby the size of the objects is gradually increased by wrapping the walks in several different ways (wrapping triangles, wrapping hexagons, and wrapping rhombuses), has also been investigated in triangular lattices [41,42]. The obtained results demonstrate that the symmetry properties of the shapes determine the kinetics of the late stage of deposition. Kondrat [43] studied the effect of the temperature on the flexibility of chains adsorbed onto a triangular lattice. Several temperature regimes were identified and discussed.

In all of the above cases, identical (monodisperse) objects or mixtures of a few shapes were considered in the deposition process. However, if the number of available configurations of the depositing objects increases, the statistical problem becomes exceedingly difficult. For example, this is the case of polymer chains generated by a self-avoiding random walk (SAW) on the lattice [44], whose treatment is still limited. Along this line Wang and Pandey [45] studied the dependence of coverage on time in a RSA of SAW chains on square lattices. Using a highly efficient event-driven algorithm [26,46], the authors found that (1) the jamming coverage decreases with the chain length and (2) it is not clear *a priori* that the jamming coverage goes to zero as the size k tends to infinity. The percolation of SAW k-mers on 2D lattices has also been studied [47–50]. The percolation analysis does not require an accurate determination of the jamming coverage.

Although the RSA problem of SAW k-mers is less developed than the corresponding RSA problem of simple objects, the experimental evidence has shown that the adsorbed molecules can, in many cases, be modeled as SAW chains of k single units. Large polymers and proteins are examples of adsorbates that can be well described by SAW configurations [51–53]. In this context, the main objectives of this paper are (1) to develop a numerical strategy to obtain the full-time kinetics of the surface coverage for structured objects deposited on discrete lattices; (2) to identify the different time regimes that can be observed during the deposition process; (3) to calculate the jamming coverage; (4) to verify the proposed method by comparing with (a) exact results for linear k-mers on one-dimensional (1D) lattices [54,55], (b) MC results for linear k-mers on 2D lattices [17,20,22,23], and (c) MC results for SAW chains on square lattices [45]; (5) to apply the proposed method to determine the dependence of θ_j with the size k for the RSA problem of SAW k-mers on honeycomb and triangular lattices; and (6) to discuss the general behavior of $\theta_{j,k}$ for SAW k-mers on 2D lattices.

The present work is a natural extension of our previous research in the area of the RSA model, and the method developed here could be applied to study irreversible adsorption of proteins and other complex molecules characterized by the wide polydispersity of their adsorption configurations. The paper is organized as follows: the model and and basic definitions are given in Sec. II. The results are presented in Sec. III. Finally, the conclusions are drawn in Sec. IV.

II. MODEL AND BASIC DEFINITIONS

The surface is represented by a honeycomb, square, or triangular lattice of $M = L \times L$ adsorptive sites, with lattice constant a and periodical boundary conditions. Initially, the lattice is completely empty. Then, particles composed by k identical units (each one occupying a lattice site) are sequentially, randomly, and irreversibly deposited following a RSA process [4]. The depositing objects are called "tortuous k-mers," and its structure is modeled as a SAW [44]. As mentioned in Sec. I, the RSA deposition leads to a blocked configuration in which no more objects can be deposited due to the absence of free space of appropriate size and shape; this blocking configuration is known as jamming state.

The irreversible deposition of structured objects on solid surfaces can be simulated as successive self-avoiding random walks on lattices. A common approach consists in randomly choosing a lattice site from which a k-step self-avoiding random walk is performed and, if all the k visited sites are empty, a SAW k-mer is deposited. If any of the sites is occupied, the attempt is rejected. One unit time in the deposition procedure (or Monte Carlo step, MCS) corresponds to L^2 repetitions of the elemental step (L^2 deposition attempts). Figure 1 shows k-mers (with $k = 4$) deposited on honeycomb [Fig. 1(a)] and square [Fig. 1(b)] lattices, and k-mers (with $k = 3$) on triangular [Fig. 1(c)] lattices. Black spheres, joined by thick lines,

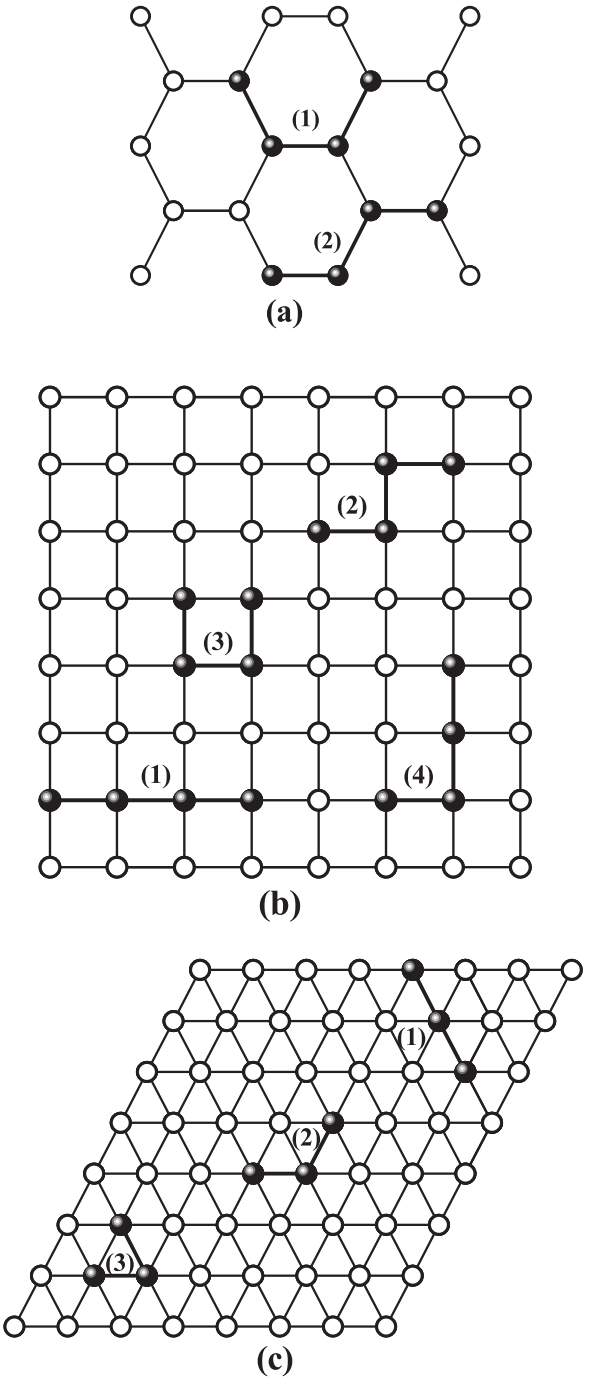

FIG. 1. (a) Available configurations for tetramers ($k = 4$) adsorbed on honeycomb lattices. (1) and (2) correspond to U-shaped and step-shaped, respectively. Black spheres, joined by thick lines, represent adsorbed k-mer units. Open circles correspond to empty sites. (b) The same as part (a) for tetramers ($k = 4$) adsorbed on square lattices. (1), (2), (3), (4) correspond to linear, step-shaped, U-shaped, and L-shaped tetramers, respectively. (c) The same as (a) for trimers ($k = 3$) adsorbed on triangular lattices. (1), (2), (3) correspond to linear, 120°, and 60° trimers, respectively.

represent adsorbed k-mer units. Open circles correspond to empty sites.

Repeating the elemental step, the particles are sequentially deposited. The surface coverage θ is defined as $\theta = kN/M$ (N is the number of the deposited k-mers), and the goal is to find the jamming coverage. This "attempt-reject" scheme is widely used to study percolation and jamming properties of linear k-mers. However, this mechanism becomes inefficient when dealing with tortuous k-mers and is very time consuming as coverage and particle size increase. In order to cope with these difficulties, we introduce an efficient rejection-free algorithm based on an systematic search of available states for deposition.

An alternative deposition scheme consists of creating an exhaustive list of all possible k-uples (sets of k empty sites) where a SAW object could be deposited. This can be achieved with an algorithm capable of tracing (in a recursive way) all the possible SAWs of k steps starting from a given site. The procedure is repeated for every site in the lattice. Once the list is built, the following steps are carried out: (1) a random k-uple is chosen from that list and is occupied by a k-mer; (2) at each step, the list is updated by eliminating all the k-uples that shared a common site with k-uple selected in (1); and (3) the process is repeated until the list is emptied.

This rejection-free algorithm provides a true jamming final state in which no other object can be deposited. The weakness of this method is the amount of memory needed to manage the list. Note that for an empty square lattice of L^2 sites, the number of configurations in the list (memory usage) rises from $18L^2$ (7 MB) for $k = 4$ to $120\,292L^2$ (1.2 TB) for $k = 12$ and $2\,374\,444L^2$ (47 TB) for $k = 15$ (the memory data were calculated using a modest ratio of $L/k = 40$). This task is illustrated in Fig. 2 for the case of tetramers ($k = 4$) on square lattices. The initial site (head) is shown as an empty circle, and the tail is represented by full circles with a gray background (from light to dark). There is a total of 18 distinguishable SAW configurations in the case of the figure.

In Ref. [45] the growth of coverage in a RSA of SAW chains on a square lattice was studied. The authors observed that the coverage rapidly increases in the short-time regime, and then because of the large number of conformational states of SAW chains, the deposition becomes very slow in the long time. Thus, in the late stage, an event-driven method [26,46] was used to speed up the simulation by identifying partial chains available for deposition.

Following the line of Ref. [45], a mixed algorithm is proposed here combining two stages: a first one of "brute-force" search (acceptance-rejection algorithm) plus a second one of "systematic search" (rejection-free algorithm). In this way, the memory limitations of the second stage can be overcome by preceding the systematic search with a limited number of steps of the standard RSA process. With this strategy, the initial size of the rejection-free list is drastically reduced. The complete algorithm is as follows. First, k-mers are deposited according to the acceptance-rejection scheme until a certain time t_1 at which the ratio between rejections and successful attempts exceeds a cutting parameter, R_C. The second stage of the deposition process consists in an exhaustive search by using the rejection-free algorithm. This stage starts from the final configuration reached in the first stage, which is expected to be relatively close to the jamming condition.

The whole process (first and second stages) guarantees to reach, in a significantly shorter computational time, a true

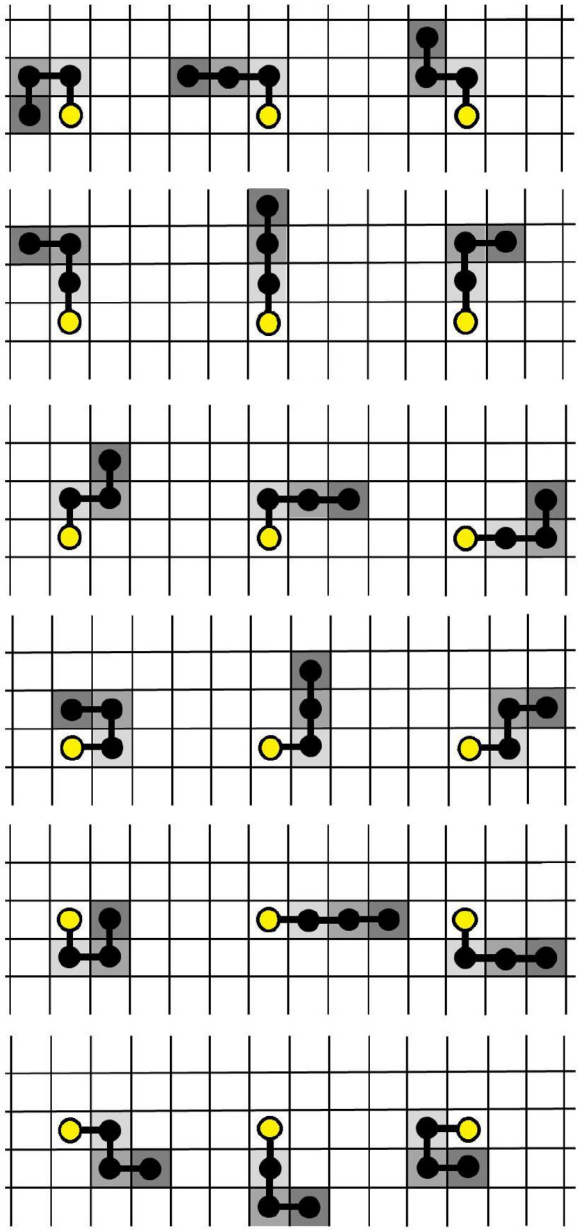

FIG. 2. Example of systematic generation of SAW configurations with $k = 4$ in the square lattice. The initial site (head) is showed in yellow, and the tail is represented by gray (from light to dark).

jamming state in which no more k-mers can be adsorbed due to absence of free space of appropriate size or shape. The developed strategy replaces the computational time consumption of the usual RSA algorithms (acceptance-rejection algorithm, stage 1) by memory consumption to allow the management of the list in stage 2 (rejection-free algorithm). The choice of the parameter R_C is of some importance, although it is not crucial. For k sizes between 2 and 9, we set R_C in the range 10^1–10^3, and the jamming configurations are reached in a reasonable time. As k is increased above $k = 9$, we set $R_C = 10^4$ to avoid having memory usage problems in the second stage.

In order to illustrate how the two-stage method works, we analyze in detail the dependence on time of the surface coverage θ for one sample corresponding to SAW chains with $k = 13$ on a square lattice with $L = 1300$. The results are shown in Fig. 3. During the first stage, Fig. 3(a) shows how the surface coverage θ increases asymptotically as a function of the simulation time t. This is because the rejection rate of the algorithm grows as the lattice is increasingly covered. In this stage the time increment for each elementary step of acceptance or rejection is $\Delta t = 1/L^2$, that is, the unit time corresponds to L^2 attempts of the standard RSA algorithm. We establish a maximum for the acceptance-rejection ratio, and, once this maximum is reached, the first stage is finished. This occurs at time $t_1 \approx 74$ MCSs, as can be seen at the end of the curve in Fig. 3(a). The value of the surface coverage after stage 1 is $\theta_1 = \theta(t = t_1) = 0.66409$.

The second stage begins by first building the exhaustive list of all the possible SAWs of k steps that can be located in the available empty sites. In this manner, the list of all possible SAWs that can be deposited on the lattice is obtained. It is worth mention that the size of this list can easily get too large if the starting configuration is not close enough to a final (jamming) condition. There is a compromise between how long the first stage is (time consuming) and the initial size of the list (amount of memory) that can be handled.

From now on, the second stage proceeds by choosing at random a SAW configuration from the list. Then the selected SAW configuration is occupied and removed from the list. At this point, any other configuration that shares sites with the selected one is also removed from the list, since these configurations are not longer possible to be occupied. Thus, the list is reduced and the process continues until the list is empty. As a result of this, we obtain a true jamming state, that is, a configuration where there is no possibility of accommodating any other SAW chain of k units.

Since the second stage guarantees that at each step a new SAW chain is deposited (there is no rejection), the coverage increases linearly with the steps [left axis and solid circles in Fig. 3(b)], unlike the asymptotic behavior observed for the coverage in the first stage [Fig. 3(a)].

Figure 3(b) shows also the evolution of the size of the list over simulation time. For this purpose, the number of remaining k-uples in the list N_R (open orange circles) is plotted as a function of the number of steps on the right axis (in logarithmic scale). At the beginning, for each SAW that is randomly selected for occupation, the number of SAWs removed from the list is very large. Towards the end, this number decreases, and the list size decreases slowly. After 13 559 steps, the list is completely empty and a jamming state is reached. In the case of the figure, $\theta_j = 0.74969$.

In order to maintain the same dynamics, and as is standard in n-fold way-like algorithms [26,45,46,56], the time increment per step in the second stage does not simply advance the time by $\Delta t = L^{-2}$ as before, but by an amount $\Delta t = (1/R)\log(1/\xi)$, where R is the ratio N_R/Z_k^{SAW}. Here N_R is again the (number of) remaining k-uples in the list, i.e., the number of potentially available k-uples to be occupied, whereas Z_k^{SAW} is the number of SAWs of k steps starting from a certain point, which could be obtained numerically. Finally, ξ is an uniformly distributed random number between 0 and 1.

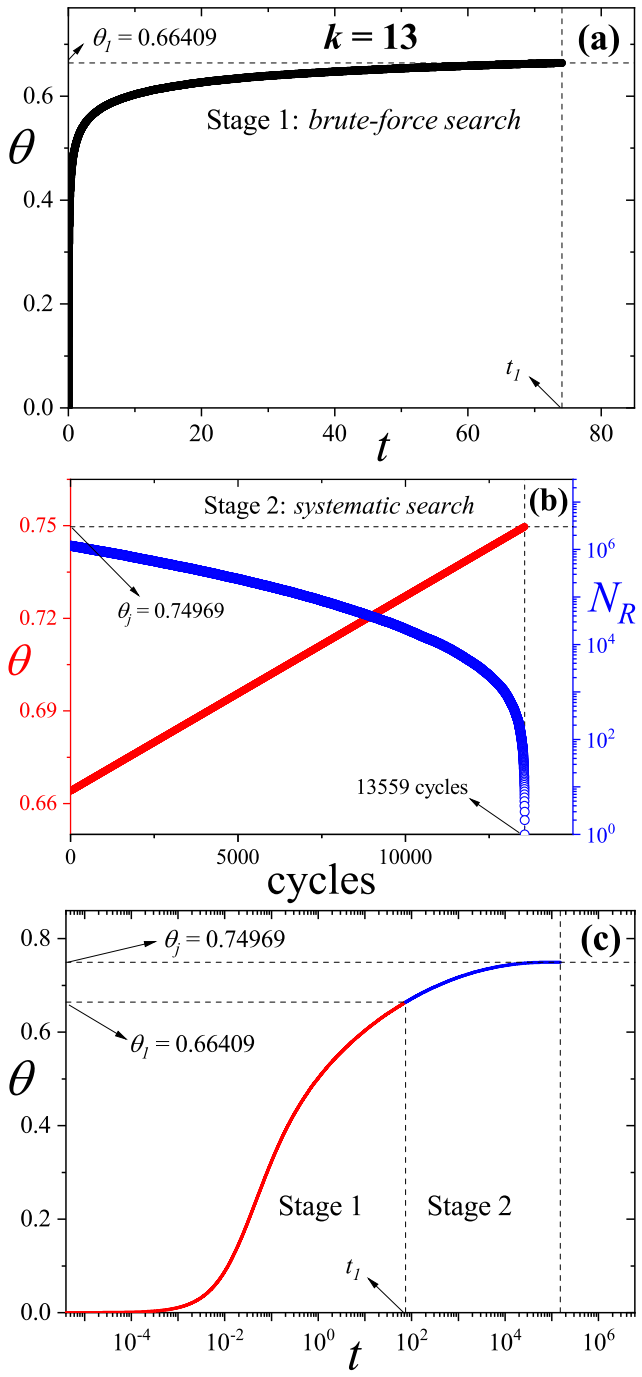

FIG. 3. (a) Surface coverage θ as a function of time t (solid black circles) for one sample corresponding to SAW k-mers with $k = 13$ deposited on a square lattice with $L = 1300$. The results were obtained by following the acceptance-rejection deposition scheme presented in Sec. II (stage 1) with $t_1 \approx 74$ MCSs. The value of the surface coverage after stage 1 [$\theta_1 = \theta(t = t_1)$] is indicated. (b) Surface coverage θ (left axis, solid red circles) and remaining k-uples in list N_R (right axis, open blue circles) as a function of the number of steps for the same case in (a). The data were obtained by following the rejection-free deposition scheme presented in Sec. II (stage 2). The value of the jamming coverage (θ_j) is indicated. (c) Surface coverage θ as a function of time t (θ axis in linear scale, t axis in log scale) for the same sample shown in (a) after the complete deposition process. The red (blue) line represents results obtained in stage 1 (2).

In Fig. 3(c) the complete time evolution of the surface coverage θ as a function of time t is shown in a semilogarithmic scale (θ axis in linear scale, t axis in log scale). The red (blue) line represents results obtained in stage 1 (2).

The procedure described in this section can be visualized in a video available in the Supplemental Material [58]. Video S1 corresponds to the deposition dynamics, corresponds to stage 1 (or "brute-force search") followed by stage 2 (or "systematic search"). At the moment of passing from stage 1 to stage 2, the work of the search algorithm for SAWs (shown in yellow) can be seen. These SAWs will form the list needed for the second stage. The configurations shown in Video S1 have been obtained for square lattices with $k = 15$ and $L = 80$, which are appropriate for illustrative purposes.

III. RESULTS

This section is organized in two parts. First, the two-stage algorithm described above is used to calculate the jamming coverage for SAW k-mer deposition onto hexagonal, square, and triangular lattices (whose connectivity is $c = 3, 4$, and 6, respectively). Second, the technique is applied to study the time evolution of the surface coverage (kinetics of packing growth) for the same systems (SAW k-mers on hexagonal, square, and triangular lattices).

The performance of the algorithm was tested by comparing the jamming value for linear k-mers with different sizes deposited onto 1D and 2D lattices obtained through the two-stage algorithm and the previously reported values [17,20,22,23,54,55]. The comparison showed a good correspondence between the two sets of values; for further details see the Appendix.

A. Tortuous k-mers

We begin studying the dependence of the jamming coverage on the size of the deposited objects for a system of SAWS irreversibly deposited on 2D lattices. Following the scheme presented in Sec. II, extensive computer simulations were developed for k ranging between 2 and 15. For each size k, 10^5 different samples were used to obtain the average jamming coverage.

The numerical results strongly depend on the finite size $M = L \times L$ of the calculation lattice. The situation can be clearly visualized in Fig. 4, where the jamming coverage $\theta_{j,k}$ is shown versus the lattice size L/k for a typical case of tortuous k-mers adsorbed on a square lattice: $k = 5$. The error bars are included in the graph. From a simple inspection of the figure it is observed that the simulation predictions improve as the lattice size increases. In our study, we used lattice sizes $L/k = 200$ ($k \in [2, 9]$) and $L/k = 100$ ($k \in [10, 15]$). With these values of the parameters, very accurate measurements of the jamming thresholds can be obtained with reasonable computational effort. The results are shown in Fig. 5 and collected in Table I (triangular lattice, second column; square lattice, third column; and honeycomb lattice, fourth column). Statistical errors on the last digits are indicated by the numbers in parentheses.

As is standard in the literature [17,22], the simulation data can be fitted to the function $\theta_{j,k} = A + B/k + C/k^2$ ($k \geqslant 2$).

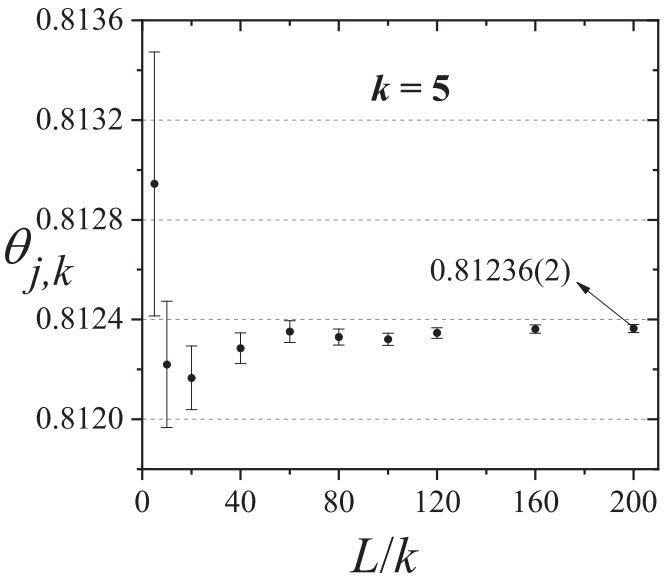

FIG. 4. Jamming coverage $\theta_{j,k}$ vs the lattice size L/k for SAW k-mers adsorbed on a square lattice and $k = 5$. The error bars are included.

In the case of Fig. 5,

$$\theta_{j,k} = A + \frac{0.75(5)}{k} + \frac{-0.65(3)}{k^2}, \tag{1}$$

where the value of A represent the limit concentration by infinitely long k-mers and depends on the connectivity of the lattice. For the cases shown in Fig. 5 $\theta_{j,k\to\infty} = 0.675(4)$ (honeycomb lattice), $\theta_{j,k\to\infty} = 0.687(5)$ (square lattice), and $\theta_{j,k\to\infty} = 0.706(3)$ (triangular lattice).

As in the case of linear k-mers on square lattices [17], the jamming coverage of tortuous k-mers on square lattices shows a decreasing behavior as a function of k, with a finite value of saturation in the limit of infinitely long k-mers. However, the $\theta_{j,k\to\infty} = 0.686(5)$ for tortuous k-mers is higher than the value $\theta_{j,k\to\infty} = 0.660(2)$ obtained for linear k-mers on square lattices [17]. It means that linear k-mers are less effective in filling the lattice than tortuous k-mers. The same behavior it is found for the triangular and honeycomb lattices where the jamming thresholds drops from $\theta_{j,k\to\infty} = 0.706(3)$ (tortuous) to $\theta_{j,k\to\infty} = 0.5976(5)$(linear [22]) and from $\theta_{j,k\to\infty} = 0.675(4)$ (tortuous) to $\theta_{j,k\to\infty} = 0.6007(6)$ (linear [23]), respectively. When tortuous k-mers are considered, the jamming threshold takes higher values as the connectivity of the lattice grows for the whole range of k. This means that, as the connectivity grows, it is easier for the tortuous k-mers to fill the lattice. The latter is not trivial since previous results on jamming for linear k-mer showed that the jamming threshold for the square lattice takes higher values than the corresponding ones for the triangular lattice (see Fig. 8).

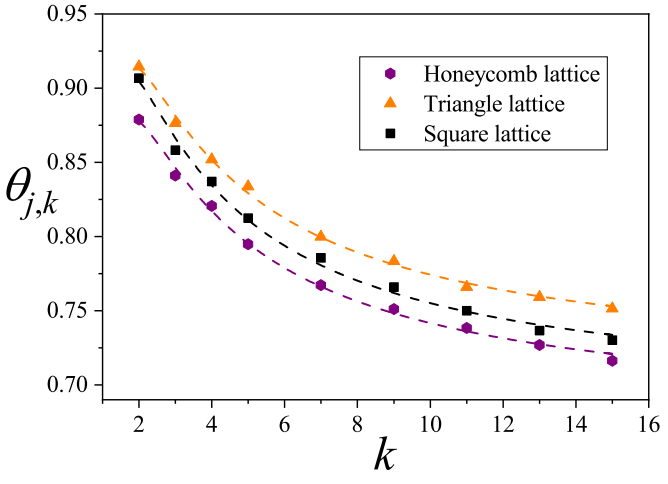

FIG. 5. Jamming coverage $\theta_{j,k}$ as a function of k for tortuous k-mers on honeycomb (hexagons), square (squares), and triangular (triangles) lattices. Symbols represent simulation results, and dashed line corresponds to the fitting function.

TABLE I. Simulation values of $\theta_{j,k}$ for tortuous k-mers on 2D lattices.

	Tortuous k-mers on 2D lattices		
k	$\theta_{j,k}$Triangular	$\theta_{j,k}$ Square	$\theta_{j,k}$ Honeycomb
2	0.91452(2)	0.90680(1)	0.87894(2)
3	0.87650(1)	0.85829(2)	0.84111(3)
4	0.85201(2)	0.83705(2)	0.82061(2)
5	0.83369(2)	0.81236(2)	0.79483(4)
7	0.79985(1)	0.78564(6)	0.76721(3)
9	0.78338(3)	0.76590(9)	0.75120(2)
11	0.76601(5)	0.75006(5)	0.73838(2)
13	0.75914(5)	0.73654(4)	0.72688(5)
15	0.75145(2)	0.73012(6)	0.71630(2)

In Ref. [45] the authors studied the RSA kinetics of self-avoiding walk chains on a square lattice and found that the jamming coverage decreases with the chain length according to a power law. By means of a highly efficient MC algorithm they were able to obtain, as here, true jamming values in reasonable simulation times. Table II collects the jamming values from [45] and the ones obtained here for the square lattice. As can be seen, both results are in good agreement within the statistical error for the interval [2,7]. In the case of $k = 15$ our result is around 5% higher than the one reported; due to the statistical differences in both studies (for $k = 15$ we use $L = 1500$ and 10^5 averages, and in [45], $L = 500$ and 700 averages), the result presented here is expected to be more accurate.

B. Kinetics of packing growth

We now analyze the time evolution of the surface coverage for SAW k-mers. As an example, the results obtained

TABLE II. Simulation values of $\theta_{j,k}$ for tortuous k-mers on the square lattice.

	Tortuous k-mers on square lattices	
k	$\theta_{j,k}$ Ref. [45]	$\theta_{j,k}$ Square
2	0.906820(2)	0.90680(1)
3	0.858296(4)	0.85829(2)
4	0.837055(13)	0.83705(2)
5	0.81235(2)	0.81236(2)
7	0.78558(1)	0.78564(6)
15	0.70178(2)	0.73012(6)

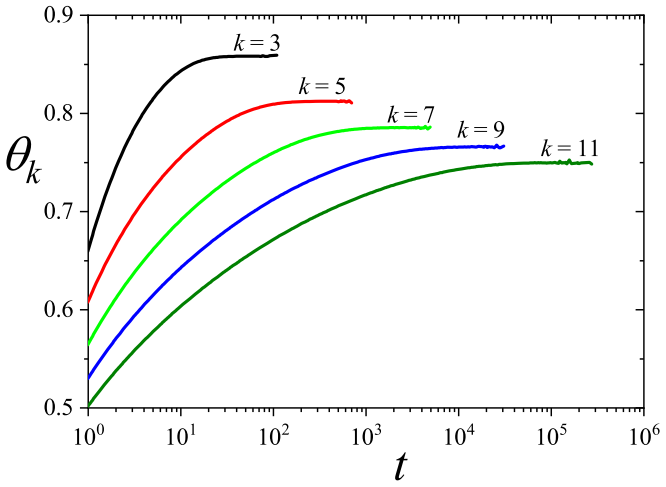

FIG. 6. Surface coverage as a function of time for tortuous k-mers on square lattices. The curves have been obtained for different values of k as indicated.

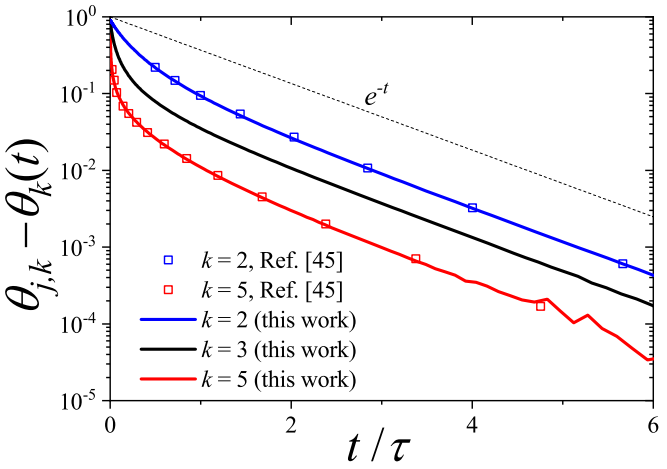

FIG. 7. Semilogarithmic plot for the difference between jamming coverage and coverage at time t for square lattices and different chain lengths as indicated. For a better view of all the curves on the same plot, we plotted again the normalized time t/τ. The dashed line is the pure exponential decay $\exp(-t)$ for $k = 1$. The value of τ was selected following the theoretical prediction in Eq. (3). Solid lines correspond to our results, and square symbols correspond to previous results in Ref. [45].

for square lattices and various chain lengths are presented in Fig. 6. The simulations are the same that were used in Sec. III A to calculate the jamming coverage. As reported in Ref. [45], a rapid increase in the coverage is observed in the short-time regime. This is followed by a very slow growth in the long time. The whole behavior can be divided into three time regimes: (1) the short-time regime, (2) the intermediate regime, and (3) the very late-stage regime. Similar behavior is obtained for triangular and honeycomb lattices.

Our interest is to study the very long-time regime. In this stage, the dynamics is controlled by filling independently the last holes, and the approach to the jamming coverage follows an exponential law in lattice deposition models [27,57],

$$\theta_{j,k} - \theta_k(t) \propto \exp\left[-t/\tau(k)\right], \tag{2}$$

where $1/\tau(k)$ is the probability that a given hole is being filled (in unit time), and [45]

$$\tau(k) = \frac{Z_k^{\text{nrrw}}}{2} = \frac{c}{2}(c-1)^{k-2}, \quad k > 1. \tag{3}$$

Z_k^{nrrw} is the number of nonreversal random walk chains of length k, and, as defined at the beginning of this section, c is the lattice connectivity: $c = 3$, hexagonal lattice; $c = 4$, square lattice; and $c = 6$, triangular lattice.

The asymptotic regime is shown in Fig. 7 for $k = 2, 3, 5$ and square lattices. The values of τ used in the plots were obtained from Eq. (3): $\tau = 2$, $k = 2$; $\tau = 6$, $k = 3$; and $\tau = 54$, $k = 5$. The figure also includes previous results from [45] for $k = 2$ and $k = 5$ (open squares). An excellent agreement is found between our data and the predictions in Ref. [45].

The analysis in Fig. 7 was repeated for other values of k and other geometries (honeycomb and triangular). In all cases the simulation results confirm the theoretical predictions in Eqs. (2) and (3). These findings validate the use of the two-stage algorithm to study the the kinetics of deposition of extended objects. Future research will be devoted to the application of the proposed method to investigate SAW deposition on more complex lattices.

IV. CONCLUSIONS

Random sequential adsorption of extended objects deposited on 2D regular lattices has been studied by numerical simulations. For this purpose, a computational scheme to determine jamming thresholds has been introduced. The proposed method is a hybrid approach that combines two stages: "brute-force search" (acceptance-rejection algorithm) and "systematic search" (rejection-free algorithm).

First, objects are sequentially deposited according to a standard acceptance-rejection scheme until a certain time t_1 at which the ratio between rejections and successful attempts exceeds a cutting parameter. The second stage of the deposition process consists of an exhaustive search of available states for deposition by using an efficient rejection-free algorithm. This stage starts from the final configuration reached in the first stage, which is expected to be relatively close to the jamming condition. The whole process (first and second stages) guarantees to reach (in a reasonable computational time) a true jamming state in which no more objects can be adsorbed due to absence of free space of appropriate size or shape.

First, the case of straight rigid k-mers was tested with analytical exact results obtained for 1D chains [54] and previous simulation data for 2D regular lattices [17,20,22,23]. An excellent agreement was observed in the comparison study, validating the applicability and accuracy of the MC method introduced here.

Second, the analysis was extended to the more interesting and complex case of tortuous k-mers deposited on honeycomb, square, and triangular lattices. The depositing objects were modeled as self-avoiding walks of k lattice steps. The jamming coverage dependence on the k-mer size was reported. On the basis of the behavior of θ_j versus k in the range $2 \leqslant k \leqslant 15$, and the best fit to this curve, the expression $\theta_{j,k} = A + B/k + C/k^2$ was obtained, where $B = 0.75(5)$ and

TABLE III. Simulation and theoretical values of $\theta_{j,k}$ for straight rigid rods on 1D lattices.

	Linear k-mers on 1D lattices	
k	$\theta_{j,k}$ [Eq. (A1)]	$\theta_{j,k}$ (Simulation)
2	0.8646647168	0.86466(4)
3	0.8236529632	0.82365(5)
4	0.8038934799	0.80389(6)
5	0.7922759137	0.79228(7)
6	0.7846301559	0.78463(7)
7	0.7792175929	0.77922(6)
8	0.7751848332	0.77519(6)
9	0.7720640600	0.77206(6)
10	0.7695774160	0.76958(6)
12	0.7658640911	0.76586(8)
14	0.7632239548	0.76323(8)
16	0.7612505524	0.76125(9)
18	0.7597196571	0.75973(9)
20	0.7584974456	0.75849(8)
100	0.74976335	0.74975(64)

$C = 0.65(3)$ are found to be shared parameters by the three lattices, and $A = \theta_{j,k\to\infty}$ represents the limit coverage by infinitely long k-mers: $\theta_{j,k\to\infty} = 0.675(4)$ (honeycomb lattice), $\theta_{j,k\to\infty} = 0.685(5)$ (square lattice), and $\theta_{j,k\to\infty} = 0.706(3)$ (triangular lattice). In the case of square lattice, the obtained jamming values agree very well with corresponding ones reported in Ref. [45]. In the case of honeycomb and triangular lattices, the behavior of θ_j as a function of k for tortuous k-mers is presented here for the first time.

Two important conclusions can be extracted from the study of the jamming properties of tortuous k-mers: (1) the functionality of θ_j vs k (given by parameters B and C) does not depend on lattice connectivity and (2) the value of the critical coverage for particles with k tending to infinity tends to a nonzero value. However, more simulations are necessary in order to confirm this tendency for large values of k and other space dimensions $d > 2$.

The full-time kinetics of the surface coverage $\theta_k(t)$ was also investigated. Three different time regimes were identified: (1) the short-time regime, (2) the intermediate regime, and (3) the very late-stage regime. Special interest was devoted to the study of the very long-time regime, where the law $\theta_{j,k} - \theta_k(t) \propto \exp[-t/\tau(k)]$ [with $\tau(k) = Z_k^{\mathrm{nrrw}}/2$] was confirmed for the three studied geometries. In the case of square lattices, our results showed an excellent agreement with those of Wang and Pandey [45], validating the two-stage algorithm to adequately keep track of time control.

The proposed scheme is simple and seems to be a promising way toward the description of irreversible adsorption of structured objects. Further applications to more complex RSA problems would in principle be feasible. In this sense, future efforts will be directed in two main directions: (1) extending the present analysis to other d-dimensional hypercubical lattices ($d > 2$), fractals, random graphs, and multilayer (and layer-by-layer) deposition and (2) analyzing the applicability of the model to interpret experimental data of protein activity in some well-known systems [52].

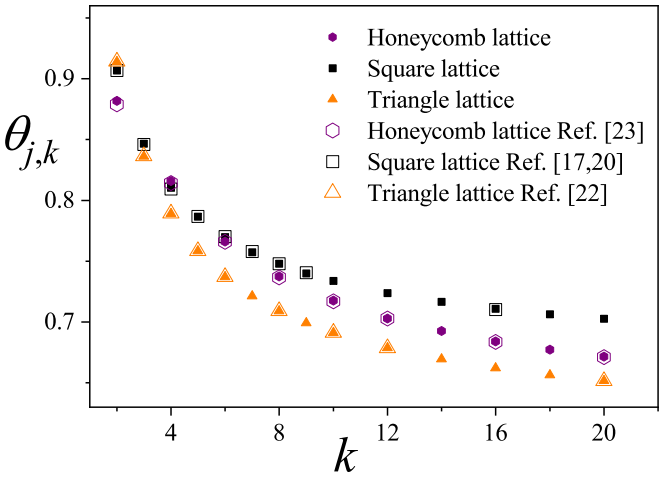

FIG. 8. Jamming coverage $\theta_{j,k}$ as function of k for linear k-mers on honeycomb (hexagons), square (squares), and triangular (triangles) lattices with k between 2 and 20. Solid symbols correspond to results obtained in this work, and open symbols to data previously reported in the literature as indicated.

ACKNOWLEDGMENTS

This work was supported in part by CONICET (Argentina) under Project No. PIP 112-201701-00673CO and Universidad Nacional de San Luis (Argentina) under Project No. 03-0816. L.S.R. acknowledges support from projects PACSS (reference RTI2018-093732-B-C22), APASOS (reference PID2021-122256NB-C21), the Maria de Maeztu Program for units of Excellence in R&D, grant CEX2021-001164-M/10.13039/501100011033, and the Juan de La Cierva program (reference FJC2021-046559-I) funded by MCIN/AEI/10.13039/501100011033 and European Union NextGenerationEU/PRTR.

APPENDIX: STRAIGHT RIGID k-MERS

As discussed in Sec. I, the complexity of the problem of irreversible adsorption of structured objects presents a major difficulty for the development of accurate analytical solutions for $\theta(t)$, and only the case of straight rigid rods (or linear k-mers) on 1D lattices has been exactly solved [54]. In this limit, $\theta(t)$ can be written as

$$\theta(t) = k \int_0^t \exp\left[-u - 2\sum_{j=1}^{k-1}\left(\frac{1-e^{-ju}}{j}\right)\right] du. \qquad \text{(A1)}$$

From Eq. (A1), the dependence on k of the jamming coverage can be obtained (as an example, some values are shown in the first column of Table I). For $k \to \infty$, the jamming threshold tends to Rényi's parking constant $\theta_j \to c_R \approx 0.7475979202$ [55].

Taking advantage of the solution in Eq. (A1), we proceed first to obtain the jamming coverage for the 1D problem through our method in order to compare with the exact result presented in Ref. [54]. The simulations were performed using a set of $n = 10^5$ independent samples with k ranging between 2 and 100, and $L/k = 100\,000$. The obtained results, which are shown in the second column of Table III, agree to five significant figures with previous exact results.

The RSA problem of straight rigid k-mers on 2D lattices was also revisited based on our two-stage algorithm. In Fig. 8 the dependence of θ_j on the size k ($2 \leqslant k \leqslant 20$) is shown for linear k-mers on honeycomb (solid hexagons), square (solid squares), and triangular (solid triangles) lattices. The calculations were done for lattices with $L/k = 100$. In addition, $n = 10^5$ runs were carried out for each value of k (and for each type of lattice). The figure includes also similar data obtained previously in the literature: linear k-mers on 2D honeycomb lattices (open hexagons, Ref. [23]), straight rigid k-mers on 2D square lattices (open squares, Refs. [17,20]), and straight rigid k-mers on 2D triangular lattices (open triangles, Ref. [22]). The present results and those previously reported in the literature coincide within the statistical uncertainty.

The excellent agreement obtained for linear k-mers (Table III and Fig. 8) validates the applicability of the method introduced here to calculate jamming thresholds.

[1] T. L. Hill, *An Introduction to Statistical Thermodynamics* (Addison-Wesley, Reading, MA, 1960).
[2] B. Senger, J.-C. Voegel, and P. Schaaf, Colloids Surf. A **165**, 255 (2000).
[3] J. Feder, J. Theor. Biol. **87**, 237 (1980).
[4] J. W. Evans, Rev. Mod. Phys. **65**, 1281 (1993).
[5] A. Cadilhe, N. A. M. Araújo, and V. Privman, J. Phys.: Condens. Matter **19**, 065124 (2007).
[6] N. A. M. Araújo and A. Cadilhe, J. Stat. Mech. (2010) P02019.
[7] R. Zallen, *The Physics of Amorphous Solids* (Wiley, New York, 1983).
[8] J. W. Evans, D. K. Hoffman, and D. R. Burgess, J. Chem. Phys. **79**, 5011 (1983).
[9] M. Hasegawa and M. Tanemura, in *Recent Developments in Statistical Inference and Data Analysis*, edited by K. Matusita (North-Holland, Amsterdam, 1980), pp. 73–78.
[10] P. Kubala, Phys. Rev. E **100**, 042903 (2019).
[11] M. Ciesla and R. M. Ziff, J. Stat. Mech. (2018) 043302.
[12] P. Kubala, P. Batys, J. Barbasz, P. Weroński, and M. Cieśla, Adv. Colloid Interface Sci. **306**, 102692 (2022).
[13] D. E. P. Pinto and N. A. M. Araújo, Phys. Rev. E **98**, 012125 (2018).
[14] S. Kundu, N. A. M. Araújo, and S. S. Manna, Phys. Rev. E **98**, 062118 (2018).
[15] G. Palacios and M. A. F. Gomes, J. Phys. A: Math. Theor. **53**, 375003 (2020).
[16] A. Baule, Phys. Rev. Lett. **119**, 028003 (2017).
[17] B. Bonnier, M. Hontebeyrie, Y. Leroyer, C. Meyers, and E. Pommiers, Phys. Rev. E **49**, 305 (1994).
[18] G. Kondrat and A. Pękalski, Phys. Rev. E **63**, 051108 (2001).
[19] M. G. Slutskii, L. Y. Barash, and Y. Y. Tarasevich, Phys. Rev. E **98**, 062130 (2018).
[20] M. Dolz, F. Nieto, and A. J. Ramirez-Pastor, Phys. Rev. E **72**, 066129 (2005).
[21] L. Budinski-Petković, I. Lončarević, M. Petković, Z. M. Jakšić, and S. B. Vrhovac, Phys. Rev. E **85**, 061117 (2012).
[22] E. J. Perino, D. A. Matoz-Fernandez, P. M. Pasinetti, and A. J. Ramirez-Pastor, J. Stat. Mech. (2017) 073206.
[23] G. A. Iglesias Panuska, P. M. Centres, and A. J. Ramirez-Pastor, Phys. Rev. E **102**, 032123 (2020).
[24] M. Nakamura, J. Phys. A: Math. Gen. **19**, 2345 (1986).
[25] M. Nakamura, Phys. Rev. A **36**, 2384 (1987).
[26] B. J. Brosilow, R. M. Ziff, and R. D. Vigil, Phys. Rev. A **43**, 631 (1991).
[27] V. Privman, J.-S. Wang, and P. Nielaba, Phys. Rev. B **43**, 3366 (1991).
[28] G. J. Rodgers, Phys. Rev. E **48**, 4271 (1993).
[29] K. Shida, R. Sahara, M. N. Tripathi, H. Mizuseki, and Y. Kawazoe, Mater. Trans. **51**, 1141 (2010).
[30] M. C. Vieira, M. A. F. Gomes, and J. P. de Lima, Physica A **390**, 3404 (2011).
[31] I. A. Kriuchevskyi, L. A. Bulavin, Y. Y. Tarasevich, and N. I. Lebovka, Condens. Matter Phys. **17**, 33006 (2014).
[32] A. J. Ramirez-Pastor, P. M. Centres, E. E. Vogel, and J. F. Valdés, Phys. Rev. E **99**, 042131 (2019).
[33] L. Petrone and M. Cieśla, Phys. Rev. E **104**, 034903 (2021).
[34] P. Adamczyk, P. Romiszowski, and A. Sikorski, J. Chem. Phys. **128**, 154911 (2008).
[35] A. Kuriata and A. Sikorski, J. Mol. Model. **21**, 56 (2015).
[36] D. Ruth, R. Toral, D. Holz, J. Rickman, and J. Gunton, Thin Solid Films **597**, 188 (2015).
[37] L. Mao, H. H. Harris, and K. J. Stine, J. Chem. Inf. Comput. Sci. **42**, 1179 (2002).
[38] Lj. Budinski-Petković and U. Kozmidis-Luburić, Phys. Rev. E **56**, 6904 (1997).
[39] Lj. Budinski-Petković, I. Lončarević, Z. M. Jakšić, S. B. Vrhovac, and N. M. Švrakić, Phys. Rev. E **84**, 051601 (2011).
[40] Lj. Budinski-Petković, I. Lončarević, Z. M. Jakšić, and S. B. Vrhovac, J. Stat. Mech. (2016) 053101.
[41] Lj. Budinski-Petković, I. Lončarević, D. Dujak, A. Karač, J. R Šćepanović, Z. M. Jakšić, and S. B. Vrhovac, Phys. Rev. E **95**, 022114 (2017).
[42] D. Dujak, A. Karač, Lj. Budinski-Petković, Z. M. Jakšić, and S. B. Vrhovac, Eur. Phys. J. B **95**, 143 (2022).
[43] G. Kondrat, J. Chem. Phys. **117**, 6662 (2002).
[44] Edited by K. Binder, *Monte Carlo and Molecular Dynamics Simulations in Polymer Science* (Oxford University Press, New York, 1995).
[45] J.-S. Wang and R. B. Pandey, Phys. Rev. Lett. **77**, 1773 (1996).
[46] J.-S. Wang, Int. J. Mod. Phys. C **05**, 707 (1994).
[47] V. Cornette, A. J. Ramirez-Pastor, and F. Nieto, Eur. Phys. J. B **36**, 391 (2003).
[48] V. Cornette, A. J. Ramirez-Pastor, and F. Nieto, Phys. Lett. A **353**, 452 (2006).
[49] M. Pawłowska, S. Zerko, and A. Sikorski, J. Chem. Phys. **136**, 046101 (2012).

[50] M. Pawłowska and A. Sikorski, J. Mol. Model. **19**, 4251 (2013).
[51] A. Christou and R. B. Stinchcombe, J. Phys. A: Math. Gen. **19**, L357 (1986).
[52] M. Rabe, D. Verdes, and S. Seeger, Adv. Colloid Interface Sci. **162**, 87 (2011).
[53] J. M. Bahi, C. Guyeux, K. Mazouzi, and L. Philippe, Comput. Biol. Chem. **47**, 246 (2013).
[54] P. L. Krapivsky, S. Redner, and E. Ben-Naim, *A Kinetic View of Statistical Physics* (Cambridge University Press, Cambridge, 2010).
[55] A. Rényi, Sel. Transl. Math. Stat. Probab. **4**, 203 (1963) [translation from Magyar Tud. Akad. Mat. Kutató Int. Közl. **3**, 109 (1958)].
[56] F. M. Bulnes, V. D. Pereyra, and J. L. Riccardo, Phys. Rev. E **58**, 86 (1998).
[57] P. Nielaba, V. Privman, and J.-S. Wang, J. Phys. A: Math. Gen. **23**, L1187 (1990).
[58] See Supplemental Material at http://link.aps.org/supplemental/10.1103/PhysRevE.107.064106 for a video showing the procedure in Sec. II.